Nanoscale

Accepted Manuscript

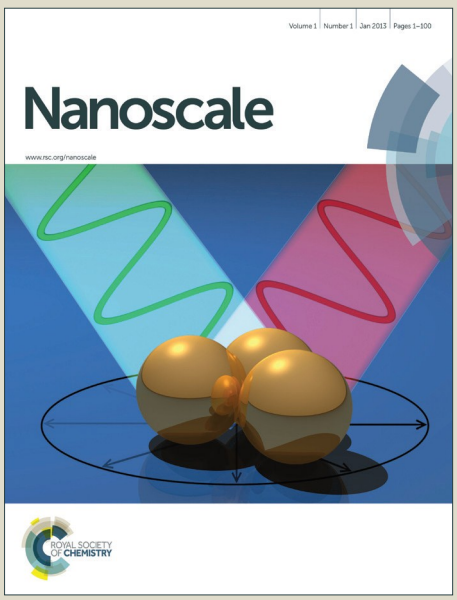

ROYAL SOCIETY OF CHEMISTRY

www.rsc.org/nanoscale

ARTICLE TYPE www. rsc.org/xxxxxx | XXXXXXXX

Transient dynamics of magnetic Co|Graphene systems

Bin Wang,[a] Jianwei Li,[a] Fuming Xu,[a] Yadong Wei,*[a] Jian Wang,*[b] and Hong Guo [c]

We report the investigation of response time of spin resolved electron traversing through a magnetic Co|Graphene nano-device. For this purpose, we calculate the transient current under step-like upward pulse for this system from first principles using non-equilibrium Green's function (NEGF) formalism within the framework of density functional theory (DFT). In the absence of dephasing mechanisms, transient current shows a damped oscillatory behavior. The turn on time of the magnetic Co|Graphene nano-device is found to be round 5∼20 femtoseconds, while the relaxation time can reach several picoseconds due to the damped oscillation of transient current for both majority spin and minority spin. The response time is determined by the resonant states below the Fermi level, but does not depend on the chirality of graphene and the amplitude of pulse bias. Each resonant state contributes to the damped oscillation of transient current with the same frequency and different decay rates. The frequency of the oscillation is the half of the pulse bias and the decay rate equals to the life time of the corresponding resonant state. When the inelastic phase-relaxing scattering is considered, the long time oscillatory behavior of transient current is suppressed and the relaxation time is reduced to hundreds of femtoseconds.

1 Introduction

Response time is one of the most important indicators to evaluate the performance of high frequency nanoscale electronic devices.[1–4] The most natural method to obtain the response time is to measure or calculate the transient current versus a sudden change of external bias. There are two typical intrinsic time scales to describe the current response, *i.e.* , the turn on time and the relaxation time.[5] The former is the time to reach the maximum current and the later measures how long the current relax to the steady state. Normally, the relaxation time is much longer than the turn on time in nanoscale systems due to the complicated quantum scattering. Several theoretical methods have been proposed to investigate the transient transport properties in nanoscales, including the real-time evolution of scattering wave function,[6,7] non-equilibrium Green's function (NEGF) methods,[8–13] NEGF within complex absorbing potentials.[14,15] Since quantum transport in realistic atomic devices is critically determined by its material property and contact geometry between device and leads, first principles investigation is necessary. To capture information of atomic details, time-dependent transport theories within the framework of density functional theory (DFT) have been proposed and applied to many simple atomic junctions, such as carbon wires, $Al-C-Al$ and $Al-DTB-Al$.[15–17] So far, the spin resolved transient dynamics in realistic magnetic electronic device has not been studied. Given the important of quantum transport in spintronic devices, it is timely to address this issue.

As a typical two dimensional material, graphene has received increasing attention due to its distinctive electronic and mechanical properties.[18–28] The weak spin-orbit interaction accompanied by long spin coherent length makes graphene a promising material for emerging spintronics.[21] Magnetism in graphene can be induced by ferromagnetic contacts,[22,23] localized dopants and defects,[24] or aryl radicals functionalization,[25] which has been investigated extensively both theoretically and experimentally. Recent experiments claimed that novel spin resolve phenomena are observed in graphene with modified surface by molecular beam epitaxy.[26] Spin-polarized transport and spin precession have been demonstrated at room temperature in graphene connected by ferromagnetic electrodes, where the polarity of spin current can be adjusted by the gate voltage and magnetic field[27,28]. Moreover, the carrier mobility in graphene is found extremely large,[18,19] showing a promising potential in ultra-fast charge transfer applications for graphene systems. Recently, graphene based field effect transistor with intrinsic cut-off frequency upon to 300 GHz has been fabricated making it a basic building block for future nanoelectronics.[1] It is the purpose of this paper to study the transient dynamics of graphene based devices.

To investigate spin resolved transient transport process in graphene nano-device, it is essential to construct a prototypical spintronic device with efficient spin injection. For this purpose, we study transport properties of a graphene based magnetic nano-device that is similar to the one used in Ref.[27], where a 2D graphene sheet is sandwiched between two magnetic metals to realize the spin injection. It has been proved that the device has large spin efficiency up to 80% and is a perfect spin filter.[27] In this paper, the spin resolved transient current is calculated using first principles method to examine the response time in such magnetic structures. We wish to address following questions in magnetic graphene systems: 1) How long is the response time of spin polarized current to a

[a] *College of Physics Science and Technology, Shenzhen University, Shenzhen, 518060, China. E-mail: ywei@szu.edu.cn; Fax: +8675526538735; Tel:+8675526535355*
[b] *Department of Physics, the University of Hong Kong, Hong Kong, China; The University of Hong Kong Shenzhen Institute of Research and Innovation, Shenzhen, China. E-mail:jianwang@hku.hk.*
[c] *Department of Physics, McGill University, Montreal, Canada.*

sudden switch-on of external pulse? 2) How does the response time depend on the magnitude of pulse bias and other parameters? 3) Does the chirality of graphene influence the current response? 4) What is the effect of phase-relaxation scattering on the response time?

First principles transient calculations are known to be extremely time consuming due to the fact that the time required to simulate transient current versus time T scales as T^3 if the wideband approximation is not used.[6,7,17] Linear scaling in T can be achieved if one uses complex absorbing potentials to replace the semi-infinite leads, reducing the computational complexity significantly.[14,15] This state-of-the-art method makes first principles transient current calculation for realistic quasi-one dimensional molecular junctions feasible.[15] For two dimensional nano-devices, however, it is very difficult to calculate transient current from first principles, even using high performance supercomputer combined with the state-of-the-art method. This is due to the fact that for 2D systems many k points has to be sampled in the first Brillouin zone in order to achieve the convergence in calculating transient current. For the graphene based magnetic nano-device studied here, it was found that more than 500 k points has to be used for the convergence of transient current making the computational time 500 times longer. To cope with this problem, we have used an approximate method which is based on the exact solution of transient current.[8] This method goes beyond the wideband approximation and has been fully tested.[16] For instance, for a quantum dot system with energy dependent self-energy due to the leads, an exact solution exists for the transient current. The transient current obtained from the approximated method agrees with that of the exact solution. The advantage of this approximated method is that it is numerically much faster and can be used for first principles transient calculation of 2D systems. Using this method we have calculated the transient current for 2D magnetic graphene systems from first principles. Damped oscillatory behaviors were observed for transient current. It was found that the long relaxation time for the transient current is due to the resonant states with long life time. In addition, the chirality of graphene and the amplitude of sudden change of bias voltage do not affect the relaxation time of the system. In the presence of dephasing mechanism, the relaxation time is suppressed from several pico-seconds to a few hundreds of femo-seconds.

This paper is organized as follows. In Sec.II, the theoretical NEGF-DFT formalism for calculating the inelastic transient currents under a step-like upward pulse is introduced which is based on the exact solution of NEGF theory. In Sec.III, the dynamic transport properties obtained from first principles are presented for two different magnetic graphene nano-devices. As a comparison, steady state transport properties are also analyzed. Finally, a summary is given in Sec.IV.

2 Theoretical formalism

According to the exact solution from NEGF theory, the transient current under an external upward pulse can be expressed as follows[29],

$$J_\alpha(t) = 2\mathrm{Re}\int \frac{d\varepsilon dk}{2\pi}\mathrm{Tr}[\mathscr{J}_\alpha(t,\varepsilon,k)] \quad (1)$$

with

$$\mathscr{J}_\alpha = A_\alpha(t,\varepsilon,k)\Sigma^{<,0}_{\alpha k}(\varepsilon) + \sum_\beta A_\beta(t,\varepsilon,k)\Sigma^{<,0}_{\beta k}(\varepsilon)F_{\beta\alpha}(t,\varepsilon,k). \quad (2)$$

Here $\Sigma^{<,0}_{\alpha k}(\varepsilon) = i\Gamma_{\alpha k}(\varepsilon - qv_\alpha)f_\alpha(\varepsilon)$ is the lesser self-energy of the device which describes the coupling between lead α and the scattering region at energy ε and wave vector k; $\Gamma_{\alpha k}$ is the line-width function of lead α at wave vector k; $f_\alpha(\varepsilon)$ is the Fermi distribution function of lead α, which is equal to 1 below the Fermi level $(E_F - qv_\alpha)$ and zero above the Fermi level at zero temperature. $A_\alpha(t,\varepsilon,k)$ and $F_{\beta\alpha}(t,\varepsilon,k)$ are functionals of time-dependent Green's functions which describe the system information and transport details; k is wave vector sampled in the first Brillouin zone of the device due to the periodicity perpendicular to the transport direction. The first term of the right-hand side of Eq.(2) describes the current flowing from lead α into the central scattering region while the second term represents the reverse process. Due to the lesser self-energy $\Sigma^{<,0}_{\alpha k}(\varepsilon)$ in Eq.(2), we see that the integration range in Eq.(1) is determined by the Fermi distribution function $f_\alpha(\varepsilon)$ and is from $-\infty$ to $E_F - qv_\alpha$. Therefore, the transient current is contributed by all the energies below the Fermi level. This is very different from the DC current where only the energy window from $E_F - qv_\alpha$ to E_F is integrated.

For an upward step-like pulse, $A_\alpha(t,\varepsilon,k)$ and $F_{\beta\alpha}(t,\varepsilon,k)$ can be obtained by the following equations which is beyond the wide-band limit[16],

$$A_\alpha(t,\varepsilon,k) = A_{1\alpha}(t,\varepsilon,k) + A_{2\alpha}(t,\varepsilon,k) \quad (3)$$

with

$$\begin{aligned} A_{1\alpha}(t,\varepsilon,k) &= \sum_n \frac{e^{i(\varepsilon-\varepsilon^0_{nk}+qv_\alpha)t}}{\varepsilon-\varepsilon^0_{nk}+i0^+}|\psi^0_{nk}\rangle\langle\phi^0_{nk}| \\ A_{2\alpha}(t,\varepsilon,k) &= \sum_n \frac{1-e^{i(\varepsilon-\varepsilon_{nk}+qv_\alpha)t}}{\varepsilon-\varepsilon_{nk}+qv_\alpha+i0^+}|\psi_{nk}\rangle\langle\phi_{nk}| \end{aligned} \quad (4)$$

and

$$[F_{\alpha\beta}(t,\varepsilon,k)]^\dagger = \Sigma^{r,0}_{\beta k}(\varepsilon)A_{1\alpha} + \Sigma^{r,0}_{\beta k}(\varepsilon - qv_\beta + qv_\alpha)A_{2\alpha}. \quad (5)$$

Here, v_α is the bias voltage of lead α and $\Sigma^{\gamma,0}_{\alpha k}(\varepsilon)$ ($\gamma = r,a,<,>$) is the self-energy of lead α in the equilibrium; $|\psi^0_{nk}\rangle$, $|\varphi^0_{nk}\rangle$ are the nth eigenstates and ε^0_{nk} is the corresponding eigenvalue

of the system in the equilibrium; $|\psi_{nk}\rangle$, $|\varphi_{nk}\rangle$ are the nth eigenstates and ε_{nk} is the nth eigenvalue of the system under non-equilibrium state. Eq.(1)-Eq.(5) form the complete set of formulae to describe the transient current in nanoscale systems for a step like upward pulse and can be implemented within the framework of density functional theory. The detailed discussion of this transient dynamic theory can be found in Ref.[16].

In the presence of ac field, the displacement current J^d_α due to the charge pileup inside the scattering region has to be considered in order to maintain the current conservation.[30] The displacement current J^d can be taken into account using the current partition method[31], from which we find that the total current I_α is given by $I_\alpha = (J_\alpha - J_\beta)/2$ which satisfies the current conservation.[32] We emphasize that this theoretical scheme of NEGF-DFT method is beyond the wideband approximation and recovers the expression of transient current obtained by Wingreen *et.al.* in the wideband limit.[33]

Note that this transient dynamic theory is based on the non-interacting model. However, when implementing the formalism (Eq.(1) to Eq.(5)) in first principles calculation, the interactions are considered within DFT where electron-electron interaction is treated on the Hartree level and the rest of the interaction is put into the exchange-correlation term. This applies to both scattering region and lead regions. As a result, the self-energy $\Sigma^{\gamma,0}_{\alpha k}(\varepsilon)$ due to the leads is also treated on the mean field level. For the upward pulse, the initial state is the equilibrium state with no bias on leads. Different exchange-correlation functional will definitely give different equilibrium potential landscape of the system and therefore different transient behavior.

3 Numerical results

To investigate spin resolved transient dynamics in graphene nano-devices, a ferromagnetic contact is essential for spin-polarized injection of electrons. Previous investigation indicated that cobalt is a good candidate for ferromagnet-graphene contact due to nearly perfect match of the lattice constants between cobalt (111) surface and graphene.[22] DC transport properties of Co|Graphene nano-device has been investigated and large spin efficiency ∼80% was reported.[27] In this paper, similar structures were built to explore the dynamic transport properties of magnetic graphene systems. Fig.1 (a)-(c) show schematic views of the Co|Graphene device, where a graphene sheet is on top of the cobalt (111) surface. Considering of the huge computational cost in the dynamic transport calculation, only three atomic layers of cobalt atoms were used to model the interface of magnetic device.[34] According to previous investigation,[22,27] the carbon atoms in A-sublattice of graphene should be located directly above the cobalt atoms and those in

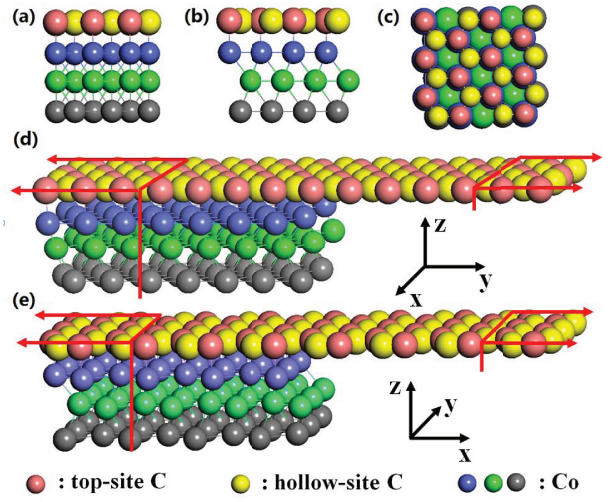

Fig. 1 (Color online) Schematic structure of periodic Co|Graphene system viewed along (a) x axis (b) y axis and (c) z axis, where a graphene sheet is put on top of the cobalt (111) surface including three atomic layers. In each panel, pink balls and yellow balls indicate the top-site and the hollow-site carbon atoms, respectively. Blue balls, green balls and grey balls indicate cobalt atoms in the first, second and third atomic layer, respectively. (d) Co|ZG system with Co|Graphene as the left lead and pristine graphene as the right lead. The system extends to $\pm\infty$ periodically along x axis and transport is along zigzag direction of graphene (y axis). (e) Co|AG system with Co|Graphene as the left lead and pristine graphene as the right lead. The system extends to $\pm\infty$ periodically along y axis and transport is along armchair direction of graphene (x axis).

B-sublattice should sit on the hollow sites (see Fig.1(c)). To obtain the most stable geometry of Co|Graphene system, total energy relaxation was done using VASP[35] by fixing the C-C bond length to 2.48 Å and relaxing the distance between each atomic layers until the force in each atom is less than 0.05 eV/Å. $8\times8\times1$ k points were sampled in the first Brillouin zone. The cut-off energy is set to be 250 Ryd and exchange-correlation energy is treated at LSDA level.[36] Fig.1 (d) and (e) show the two-probe schematic structures of the magnetic graphene nano-device, which consist of Co|Graphene as left lead and pristine graphene as right lead. In Fig.1(d), the device is extended periodically along x axis and the current is driven along y axis (zigzag direction). In Fig.1(e), the device is extended periodically along y axis and the current is driven along x axis (armchair direction). These two structures will be hereafter referred to as Co|ZG and Co|AG, respectively.

The spin resolved quantum transport properties of Co|ZG and Co|AG were investigated using the first principles package NanoDCal which is based on the standard NEGF-DFT method.[37–39] In this method, a linear combination of the atomic orbitals is employed as basis set to solve the Kohn-

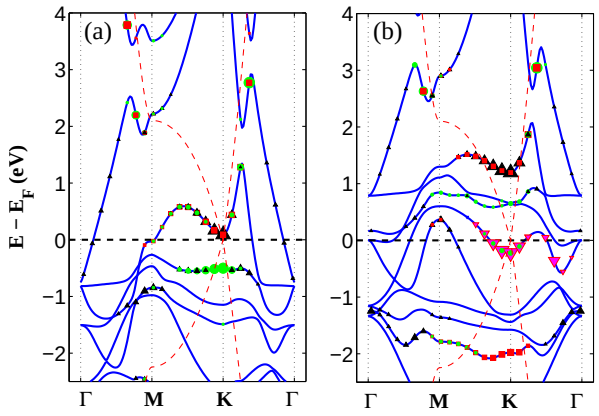

Fig. 2 (Color online) Blue solid curves: spin polarized band structures of periodic Co|Graphene interface for (a) majority spin and (b) minority spin. Red dash curves: band structure of perfect graphene. The red squares and green circles indicate the weight of p_z orbital of top-site C atoms and hollow-site C atoms, respectively. The black up-triangles and pink down-triangles indicate the weight of d_{z^2} orbital and $d_{xy}+d_{x^2-y^2}$ orbitals of top-site Co atoms, respectively. The horizontal black-dash lines describe the Fermi level.

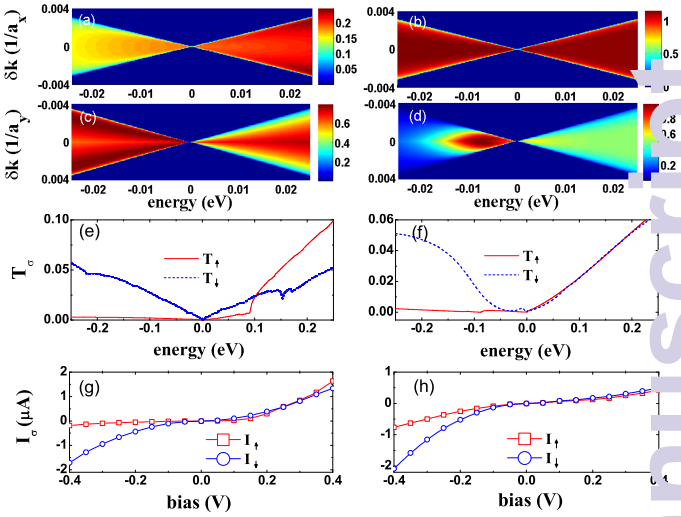

Fig. 3 (Color online) $\mathcal{T}_\sigma(E,k)$ versus energy and wave vector under equilibrium for (a) majority spin of Co|ZG system; (b) minority sp of Co|ZG system; (c) majority spin of Co|AG system ; and (d) minority spin of Co|AG system. $\delta k = k - k_0$ with k the wave vect in the first Brillouin zone and $k_0 = 0$ for Co|ZG system (panel (a) and panel (b)) and $k_0 = \pm 2\pi/3$ for Co|AG system (panel (c) and panel (d)). The units of wave vectors are $1/a_x$ and $1/a_y$, where a_x is the supercell length along x axis for Co|ZG system and a_y is the supercell length along y axis for Co|AG system. (e)-(f): $T_\sigma(E)$ versus energy under equilibrium for Co|ZG system and Co|AG system, respectively. (g)-(h): I_σ versus bias voltage for Co|ZG system and Co|AG system, respectively.

Sham equations numerically. The exchange-correlation is treated at the LSDA level[36] and a nonlocal norm-conserving pseudopotential[40] is used to define the atomic core. In our calculation, the NEGF-DFT self-consistency is carried out until the numerical tolerance of Hamiltonian matrix is less than 10^{-4}eV.

Fig.2 shows the spin polarized band structures of periodic Co|Graphene system as shown in Fig.1(a). As a comparison, the band structure of pristine graphene is also shown (red dash curves). Due to the strong coupling between cobalt surface and graphene, the linear dispersion relationship of pristine graphene at K point is destroyed for both majority spin and minority spin. To examine the influence of cobalt surface to the electronic structures of graphene quantitatively, the weight of p_z orbital of carbon atoms and d orbital of cobalt atoms to each bands is superimposed in Fig.2(a) and Fig.2(b) where the size of the symbol shows the weighting. Two special features are observed. (i) The electron-hole symmetry of pristine graphene is broken in the Co|Graphene system. For majority spin, a local band gap is opened up at K point and the Fermi velocity of spin polarized electron is decreased significantly compared to that of the pristine graphene. The flat valence band around K point indicates a vanishing velocity of the hole. For minority spin, the effective mass of electron is largely increased at K point and system shows metallic properties. (ii) The equivalence of A-B sites of pristine graphene is destroyed. For pristine graphene, conduction band and valence band are contributed equally by A-site and B-site of carbon atoms. For majority spin of Co|Graphene system, the valence band around K point is dominated by p_z orbital of hollow-site carbon atoms, while the conduction band is mostly contributed by the hybridization between p_z orbital of top-site carbon atoms and d_{z^2} orbital of cobalt atoms. For minority spin, the band around the Fermi level near K point is mostly contributed by d orbital of cobalt atoms in $x-y$ plane (d_{xy} and $d_{x^2-y^2}$). The existence of this band is due to the doping of Co atoms. There are also two bands near K point above the Fermi level which are evolved from a degenerate level of graphene during the Co doping. The upper band is contributed by top-site carbon atoms and the lower band is dominated by hollow-site carbon atoms (see red squares and green circles in Fig.2(b)). From this analysis, we see that due to the Co doping the Fermi velocity of both majority and minority spin are reduced significantly which may have implication on the response time. Moreover, we expect a suppression of transient current for majority spin due to the existence of a gap at the K point.

Now we study transport properties of our systems. For the magnetic graphene nano-devices under a given pulse bias, the magnitude of transient current should be exactly equal to the

DC current when time tends to infinity. Therefore, the steady state properties under different bias voltages are essential to understand the dynamic transport properties. Our devices are 2D systems which are periodic in the transverse direction, i.e., x direction for Co|ZG or y direction for Co|AG. The spin resolved transmission coefficient T_σ can be calculated by[41]

$$T_\sigma(E) = \int \frac{dk}{2\pi} \mathscr{T}_\sigma(E,k) \tag{6}$$

with

$$\mathscr{T}_\sigma(E,k) = \mathrm{Tr}[\Gamma_{L,k}(E) G^r_k(E) \Gamma_{R,k}(E) G^a_k(E)]_{\sigma\sigma}, \tag{7}$$

where k is the wave vector sampled in the 1D Brillouin zone; G^r_k is the retarded Green's function of the system at wave vector k and is defined as $G^r_k = [E - H_k - \Sigma^r_{L,k} - \Sigma^r_{R,k}]^{-1}$; $\Gamma_{\alpha,k} = i(\Sigma^r_{\alpha,k} - \Sigma^a_{\alpha,k})$ ($\alpha = L,R$) is the linewidth function at k point which describes the coupling between α lead and the scattering region. Under finite bias voltage, spin resolved current can be calculated using the Landauer-Bütticker formula as follows,

$$I_\sigma = \frac{q}{h} \int dE [f_L - f_R] T_\sigma(E), \tag{8}$$

where f_α is the Fermi distribution function of lead α.

According to Eq.(7), the equilibrium k-sampled transmission coefficients $\mathscr{T}_\sigma(E,k)$ close to the Fermi level were calculated and shown in Fig.3(a)-(d). For Co|ZG, $\mathscr{T}_\uparrow$ and $\mathscr{T}_\downarrow$ are nonzero only around $k = 0$, which exhibits sharp cone shapes with Fermi velocity equal to that of Graphene (see Fig.3(a) and Fig.3(b)). While, for Co|AG, $\mathscr{T}_\uparrow$ and $\mathscr{T}_\downarrow$ are nonzero only around $k = \pm 2\pi/3$ where two sharp cones appear (see Fig.3(c) and Fig.3(d)). In the other k region, $\mathscr{T}_\uparrow$ and $\mathscr{T}_\downarrow$ are all equal to zero. This phenomenon can be understood as follows. Because the right lead of the magnetic device is pure graphene, the electron can flow only through the K point of the hexagonal Brillouin zone where density states are available, although there are more bands in the left lead. Moreover, due to the presence of lead, the periodicity along the transport direction is destroyed, the 2D Brillouin zone of graphene is reduced to a 1D one perpendicular to the transport direction. For Co|ZG system, the K (or K') points of hexagonal Brillouin zone of 2D primitive graphene are folded over the Γ point of 1D Brillouin zone corresponding to $k = 0$. While for Co|AG system, the K (or K') point is located on the $\pm 2\pi/3$ along the k axis of 1D Brillouin zone. As a result, the DC transport is dominated by $k = 0$ for Co|ZG and $k = \pm 2\pi/3$ for Co|AG near and below the Fermi level. Fig.3(e) and Fig.3(f) show the equilibrium $T_\sigma(E)$ around the Fermi level for Co|ZG and Co|AG, respectively. When the energy is below 0.1 eV, $T_\downarrow$ is much larger than $T_\uparrow$ for both systems, because of the majority spin band gap around K point below the Fermi level as shown in Fig.2(a). As a result,

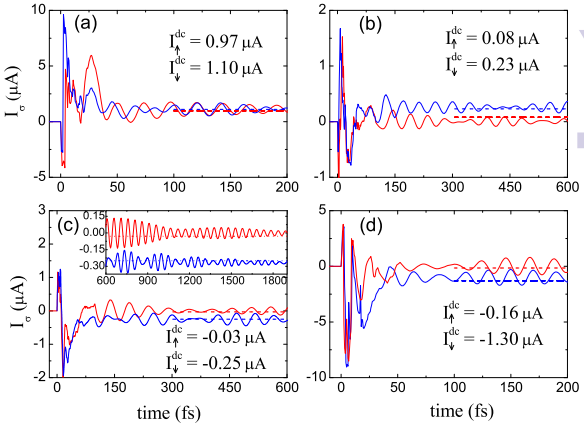

Fig. 4 (Color online) Spin polarized transient current I_σ of Co|ZG system under different pulse biases $v = v_L - v_R = 2v_L$ for (a) $v = 0.35$ V, (b) $v = 0.15$ V, (c) $v = -0.15$ V, and (d) $v = -0.35$ V. The red curves, blue curves, red dash lines and blue dash lines indicate $I_\uparrow(t)$, $I_\downarrow(t)$, $I^{dc}_\uparrow$ and $I^{dc}_\downarrow$, respectively.

$I_\uparrow$ is much smaller than $I_\downarrow$ for both systems under lower bias voltage as shown in Fig.3(g) and Fig.3(h).

Having examined the DC transport properties of magnetic graphene nano-devices, we now focus on its transient process under step-like upward pulse with different pulse biases. A sudden change of bias from zero to v_α is applied to both left (Co|Graphene) and right (pristine graphene) leads where $v_L = v/2$ and $v_R = -v/2$. Using Eq.(1), the transient currents at different upward pulse biases were calculated from first principles, where more than 10000 energy points from transmission threshold to the Fermi level were scanned in order to obtain a convergent result. For each energy, more than 500 k points in the 1D first Brillouin zone was sampled to ensure the accuracy of transient current calculation.[42] Fig.4(a)-(d) show the transient current $I_\uparrow(t)$ and $I_\downarrow(t)$ of Co|ZG system under different pulse biases. Several observations are in order. (i) Once the pulse is turned on, $I_\sigma(t)$ increases rapidly from zero to a large value in the first a few femtoseconds and then decays with oscillations to the steady state DC current. This is a general feature for all the pulse biases. (ii) For all the pulse biases, the turn-on time τ (time to reach the maximum current) is roughly 5∼20 fs for both majority spin and minority spin. Considering that the length of scattering region L of Co|ZG is about 21Å, the envelope velocity $V = L/\tau$ is roughly $1\sim4$ $Å/fs$. This value is in accordant with the Fermi velocity $V_F = 1/\hbar\partial E/\partial k$ which can be estimated from Fig2.(a) with the value about 3.5 $Å/fs$. From this velocity, we estimate the transit time to be 6 fs. (iii) The relaxation time (time from t=0 to reach to steady state) is much longer than the turn-on time due to the oscillation of $I_\sigma(t)$. Quantitatively, we define the

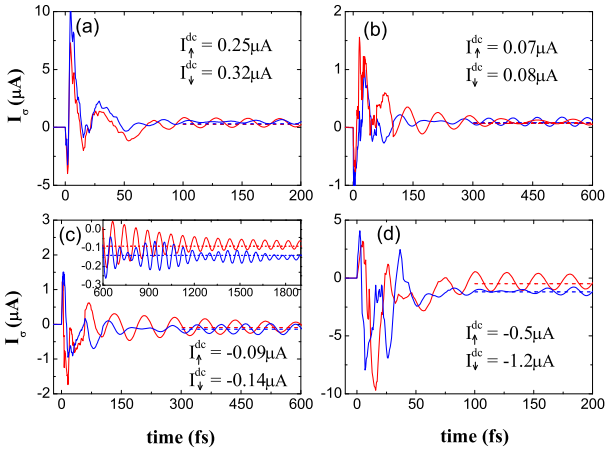

Fig. 5 (Color online) Spin polarized transient current I_σ of Co|AG system under different pulse biases $v = v_L - v_R$ for (a) $v = 0.3$ V, (b) $v = 0.1$ V, (c) $v = -0.1$ V, and (d) $v = -0.3$ V. The red curves, blue curves, red dash lines and blue dash lines indicate $I_\uparrow(t)$, $I_\downarrow(t)$, $I_\uparrow^{dc}$ and $I_\downarrow^{dc}$, respectively.

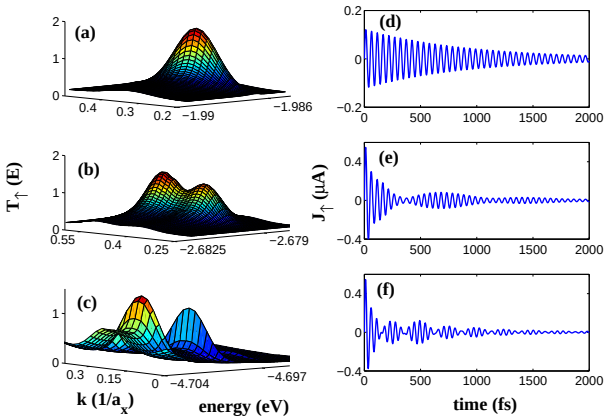

Fig. 6 (Color online) (a)-(c): Equilibrium transmission coefficient $\mathscr{T}_\uparrow(E,k)$ around special wave vector k and energy corresponding to quasi-bound states of Co|ZG; (d)-(f): The corresponding transient current $J_\uparrow(\varepsilon,k)$ of Co|ZG at $v = -0.15$ V.

relaxation time τ_r as $\kappa = 10\%$ where

$$\kappa = \frac{I_\sigma(\tau_r) - I_\sigma^{dc}}{I_\sigma^{dc}} \tag{9}$$

with I_σ^{dc} the spin polarized DC current under bias voltage v. As shown in the inset of Fig.4(c), the relaxation time can reach $\simeq 2000$ fs. The order of magnitude of these two time scales τ and τ_r are, respectively, almost the same for all the pulse biases. (iv) The oscillating frequency of $I_\sigma(t)$ can be estimated accurately and found to be proportional to the bias v so that the current is proportional to $\cos(qvt/2)$, which agrees with previous investigation.[16,33] For instance, this gives the distance between adjacent peaks $t \sim 22$ fs with $v = 0.35$ V as shown in Fig.4(a). (v) Due to the asymmetry of Co|ZG structure along the transport direction, transient currents show different behaviors under reverse biases as shown in Fig.4(a) and Fig.4(d).

Fig.5(a)-(d) show the transient current of Co|AG system under different pulse biases. Similar to Co|ZG, both majority spin and minority spin currents show damped oscillatory behaviors for all the pulse biases. We found that turn-on time and relaxation time are also about 5∼20 fs and several ps, respectively. Our results show that the response times of magnetic graphene system *do not* depend on the chirality of graphene and the amplitude of bias voltage.

According to Ref.[16], the long time oscillatory behavior of transient current is dominated by the quasi-bound states (resonant states) below the Fermi level. Due to the long life time of the quasi-bound state, an incoming electron can dwell on that state for a long time. The longer the life time of quasi-bound state is, and the slower the current decays. The quasi-bound state can be located from a sharp resonant peak of transmission coefficient with the peak width corresponding to the life time. The decay rate can also be estimated analytically. For a particular quasi-bound state with half-width of the sharp peak equal to Γ_0 around wave vector k and energy ε_{nk}, A_α in Eq.(4) is approximately $\exp(i(\varepsilon - \varepsilon_{nk}^0 + qv_\alpha)t - (\Gamma_0/2)t)$.[43] Supposing the current J_α in Eq.(1) is mostly contributed by this sharp peak, the time evolution of J_α is mostly determined by the factor of $|A_\alpha|^2$ which can be further reduced to $\exp(-\Gamma_0 t)$. Obviously, the current exhibits oscillating behavior with frequency equal to half of the strength of pulse bias v and decay rate equal to the life time of the corresponding resonant state Γ_0.

For the calculation of Co|ZG and Co|AG, more than 500 k points in the first Brillouin zone and 10000 energy points from transmission threshold to the Fermi level were scanned to resolve all the sharp resonant states. Roughly 50 quasi-bound states were found and three most contributed ones to $\mathrm{Tr}[\mathscr{J}_{L,\uparrow}(t)]$ of Co|ZG at $v = -0.15$ V are shown in Fig.6. For each quasi-bound state labeled by peak 1 to peak 3, the corresponding current obtained by integrating $\mathrm{Tr}[\mathscr{J}_{\alpha,\uparrow}(\varepsilon,k)]$ over the neighborhood of this peak is also given in Fig.6. For peak 1 in Fig.6(a), the half-width Γ_1 is roughly 4×10^{-4} eV and the corresponding relaxation time τ_{r1} should be ∼2188 fs from the expression $\exp(-\Gamma_1 \tau_{r1}) = e/10$ (from Eq.(9)), which is accordant with the numerical results shown in Fig.6(d). Peak 2 and peak 3 also give proper agreements between the half-widths Γ_2 and Γ_3 and the corresponding transient currents, respectively. Comparing to Fig.4(c), we see the contribution of peak 1 to peak 3 to $\mathrm{Tr}[\mathscr{J}_{L,\uparrow}(t)]$ is more than 70% when t>200 fs. The competition of all the quasi-bound states gives rise to the long time oscillation of the transient current.

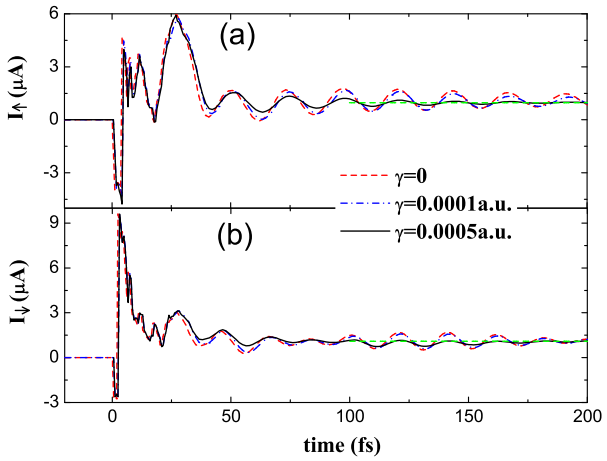

Fig. 7 (Color online) Dephasing influenced $I_{\uparrow}$ (a) and $I_{\downarrow}$ (b) of Co|ZG system with different depahsing parameters when $v = 0.35$ V. The red dash curves, blue dash-dot curves, and black solid curves indicate I_{σ} with dephasing parameter $\gamma = 0$, $\gamma = 0.0001$ a.u. and $\gamma = 0.0005$ a.u. (1 a.u. = 27.2 eV), respectively. The green lines are the values of spin resolved DC current.

So far, all the discussion about dynamic transport properties of the magnetic graphene device is in the coherent transport regime with implicit assumption that only the elastic scattering occurs for the electron and the inelastic scattering is ignored. This is reasonable at low temperatures where electron phonon coupling can be neglected.[44] However, for an actual atomic device under operational condition, temperature effect must be considered along with other inelastic scatterings. For the transient dynamics, non-zero temperature would smear out the sharp resonant peak and in turn affect the lifetime of quasi-bound states and the response of the system. To include the temperature smearing effect in our theory, the integration range in Eq.(1) must be expended which will further increase the computational complexity.

An alternative way is to include dephasing into the system which is computational less expensive. Dephasing in system is a very complex process which is related to temperature, external bias, and disorder. The main mechanism of dephasing arises from electron-phonon (e-ph) coupling in molecular tunneling junction. Experimentally, the strength of e-ph coupling can be quantified through measuring the vibrational spectrum which roughly corresponds to the peaks of the second derivative of current, *i.e.*, d^2I/dV^2.[45] Theoretically, the strength of e-ph coupling is contributed by all phonon models including both elastic scattering and inelastic scattering. Accurate value of e-ph coupling strength needs to be determined self-consistently from first principles.[46] To avoid the self-consistent calculation, some phenomenological theories have been established where e-ph coupling strength is simplified as some parameters.[47,48] It has been proved that dephasing effects calculated using phenomenological theory are in accordant with those obtained from self-consistent calculation quantitatively in molecular devices.[49] In the following we will use such a phenomenological theory developed by M. Buttiker[47] to investigate the influence of dephasing to the long time oscillatory behavior of $I_{\sigma}(t)$ for Co|ZG and Co|AG.

According to Ref.[47], the dephasing can be considered as a fictitious probe and the effect to the system is described through introducing a scattering self-energy term $\Sigma^r_{\mathrm{e-ph}}$ as follows,

$$\Sigma^r_{\mathrm{e-ph}} = -\frac{i}{2}\gamma S \qquad (10)$$

where γ is dephasing parameter which describes the strength of e-ph coupling in the device. Then the influence of dephasing to the transient current can be included qualitatively through adding the term $\Sigma^r_{\mathrm{e-ph}}$ to the self-energy of the system. In the following, we will vary the dephasing parameter to reveal the intrinsic behaviors on how the relaxation time is influenced by dephasing.

Using this method, the influence of dephasing to transient current of Co|ZG and Co|AG was investigated. Fig.7 shows $I_{\sigma}(t)$ of Co|ZG under 0.35 V pulse bias (see Fig.4(a)) with different dephasing parameters. In the first ~25fs, the current is almost not influenced by dephasing. But when t>25 fs, the oscillating amplitude of $I_{\sigma}(t)$ decreases with the increase of dephasing parameter γ. When γ is increased to 0.0005 a.u., the oscillation disappears gradually and the current decays to the steady state value after about 200 fs. That is means the relaxation time is largely reduced from several picoseconds to dozens of femtoseconds. Numerically, the quasi-bound states mainly origin from the singular points in Eq.(4) where energy is scanned in the real axis. The dephasing term $\Sigma^r_{\mathrm{e-ph}}$ gives an additional imaginary part $-\frac{i}{2}\gamma S$ to the Hamiltonian, which moves the singular points away from the real axis. As a result, the long time oscillating behavior of current is decayed approximately by the factor $\exp(-\gamma t)$. When γ=0.0005 a.u. and t=200 fs, $\exp(-\gamma t) \sim 0.016$ and the transient current almost reaches its DC limit.

More importantly, supposing dephasing in the Co|Graphene system is only induced by temperature, we can estimate the electron temperature approximately from dephasing parameter γ by $\gamma = k_B T$. So, γ=0.0005 a.u. corresponds to a low temperature ~ 158 Kelvin which is much lower than the natural operating temperature of electronic device. Numerical results show that dephasing gives quantitatively the same decay rate of the relaxation time for both Co|ZG and Co|AG under different pulse biases. Therefore, we confirm that the chirality of graphene in our Co|Graphene nano-device practically do not influence the current response time.

To improve the performance of the nano-devices it is desir-

able to eliminate these quasi-bound states that dominate the relaxation time of the system. Physically, it is known that these quasi-bound states mediate the resonant tunneling. To get rid of the resonant tunneling, in another word, to eliminate the quasi-bound state, we can dope the system whose effect is to smear out the resonant peak thereby decrease the lifetime of the quasi-bound state. We note that calculating I-V curve in the presence of doping has been formulated within NEGF-DFT framework and implemented in the static calculation from first principles.[51] However, how to use this formalism for transient calculation is still a research topic and we hope to report this progress in the near future.

4 Conclusions

In conclusion, we investigated the spin resolved dynamic transport properties of magnetic Co|ZG and Co|AG systems from first principles calculation. For both majority spin and minority spin currents, the turn on time is roughly 5∼20 fs and the relaxation time can reach several ps due to long time oscillatory behavior of transient spin current. When considering of the dephasing from e-ph inelastic scattering, the long time oscillatory behavior of I_σ disappears and the relaxation time can be reduced to $\sim$ 200 fs. The chirality of graphene and the amplitude of pulse bias do not influence the response time of magnetic graphene nano-devices.

Acknowledgments This work was financially supported by grant from the National Natural Science Foundation of China (Grant No. 11304205, 11447159, and 11374246) and Shenzhen Natural Science Foundation (JCYJ20130326111836781). J.Wang acknowledges the support from the University Grant Council (Contract No. AoE/P-04/08) of the Government of HKSAR.

References

1 L.Liao, Y.C. Lin, M.Q. Bao, R. Cheng, J.W. Bai, Y.A. Liu, Y.Q. Qu, K.L. Wang, Y. Huang, and X.F. Duan, *Nature*, 2010, **467**, 305.
2 Y.M. Lin, A. Valdes-Garcia, S.J. Han, D.B. Farmer, I. Meric, Y.N. Sun, Y.Q. Wu, C. Dimitrakopoulos, A. Grill, and P. Avouris, *Science*, 2011, **332**, 1294.
3 C. Sire, F. Ardiaca, S. Lepilliet, J. Seo, M.C. Hersam, G. Darnbrine, H. Happy, and V. Derycke, *Nano Lett*, 2012, **12**, 1184.
4 N. Petrone, I. Meric, J. Hone, K.L. Shepard, *Nano Lett*, 2013, **13**, 121.
5 J. Gabelli, G. Fève, T. Kontos, J.-M. Berroir, B. Placais, D. C. Glattli, B. Etienne, Y. Jin, and M. Büttiker, *Phys. Rev. Lett.*, 2007, **98**, 166806.
6 S. Kurth, G. Stefanucci, C.-O. Almbladh, A. Rubio, and E. K. U. Gross, *Phys. Rev. B*, 2005, **72**, 035308.
7 G. Stefanucci, E. Perfetto, and M. Cini, *Phys. Rev. B*, 2008, **78**, 075425; *ibid.*, 2010, **81**, 115446.
8 J. Maciejko, J. Wang, and H. Guo, *Phys. Rev. B*, 2006, **74**, 085324.
9 X.Q. Li and Y. J. Yan, *Phys. Rev. B*, 2007, **75**, 075114.
10 X. Zheng, F. Wang, C. Y. Yam, Y. Mo, and G.H. Chen, *Phys. Rev. B*, 2007, **75**, 195127.
11 H. Xie, F. Jiang, H. Tian, X. Zheng, Y. Kwok, S.G. Chen, C.Y. Yam, Y.J. Yan and G.H. Chen, *J. Chem Phys.*, 2012, **137**, 044113.
12 A. Pertsova, M. Stamenova, and S. Sanvito, *J. Phys.: Condens. Matter*, 2013, **25**, 105501.
13 R. Tuovinen, E. Perfetto, G. Stefanucci, and R. van Leeuwen, *Phys. Rev. B*, 2014, **89**, 085131.
14 K. Varga, *Phys. Rev. B*, 2011, **83**, 195130.
15 L. Zhang, J. Chen, and J. Wang, *Phys. Rev. B*, 2013, **87**, 205401.
16 B.Wang, Y. Xing, L. Zhang and J. Wang, *Phys. Rev. B*, 2010, **81**, R121103; Y.X. Xing, B. Wang, and J. Wang, *Phys. Rev. B*, 2010, **82**, 205112.
17 L. Zhang, Y.X. Xing, and J. Wang, *Phys. Rev. B*, 2012, **86**, 155438.
18 K.S. Novoselov, A.K. Geim, S. V. Morozov, D. Jiang, M. I. Katsnelson, I. V. Grigorieva, S. V. Dubonos and A. A. Firsov, *Nature*, 2005, **438**, 197.
19 S.V. Morozov, K.S. Novoselov, M.I. Katsnelson, F. Schedin, D.C. Elias, J.A. Jaszczak, and A.K. Geim *Phys. Rev. Lett.*, 2008, **100**, 016602.
20 K.S. Novoselov, V.I. Falko, L. Colombo, P.R. Gellert, M.G. Schwab, and K. Kim, *Nature*, 2012, **490**, 192.
21 T. Nikolaos, J. Csaba, P. Mihaita, H.T. Jonkman and B-J. van Wees, *Nature*, 2007, **448**, 571.
22 V.M. Karpan, G. Giovannetti, P.A. Khomyakov, M. Talanana, A.A. Starikov, M. Zwierzycki, J. van den Brink, Brocks, and P.J. Kelly, *Phys. Rev. Lett.*, 2007, **99**, 176602.
23 F. Donati, Q. Dubout, G. Autes, *Phys. Rev. Lett.*, 2013, **111**, 236801.
24 E. Santos, D. Sanchez-Portal, and A. Ayuela, *Phys. Rev. B*, 2010, **81**, 125433.
25 J. Hong, E. Bekyarova, P. Liang, W.A. de Heer, R.C. Haddon, and S. Khizroev, *Sci. Rep.*, 2012, **2**, 624.
26 A.G. Swartz, K.M. McCreary, W. Han, J. Wong, P.M. Odenthal, H. Wen, J.R. Chen, R.K. Kawakami, Y.F. Hao, R.S. Ruoff, and J. Fabian, *J. Vac. Sci. Technol B*, 2013, **31**, 040105.
27 J. Maassen, W. Ji, and H. Guo, *Nano. Lett.*, 2011, **11**, 151.
28 O. van t Erve, A. Friedman, E. Cobas, *Nat. Nanotech.*, 2012, **7**, 737.

29 J. Maciejko, J. Wang, and H. Guo, *Phys. Rev. B*, 2006, **74**, 085324.

30 M. Buttiker, A. Pretre, and H. Thomas, *Phys. Rev. Lett.*, 1993, **70**, 4114.

31 B.G. Wang, J. Wang, and H. Guo, *Phys. Rev. Lett.*, 1999, 82, 398.

32 A.-P. Jauho, N. S. Wingreen and Y. Meir, *Phys. Rev. B*, 1994, **50**, 5528.

33 N. S. Wingreen, A.-P. Jauho and Y. Meir, *Phys. Rev. B*, 1993, **48**, 8487.

34 Structures in this paper are similar but different from the adequately investiaged ones in Ref.[27] where graphene is sandwiched between several Co layers. The main purpose of designing such a new structure but not directly using the old one built in Ref.[27] is to reduce the computational complexity of transient current calculation which is extremely time consuming as discussed in the forth paragraph of this paper.

35 G. Kresse and J.Furthmuller, *Phys. Rev. B*, 1996, **54**, 11169.

36 U. von Barth and L. Hedin, *J. Phys. C*, 1972, 5, 1629; O. Gunnarsson and B. I. Lundqvist, *Phys. Rev. B*, 1976, **13**, 4274.

37 J. Taylor, H. Guo and J. Wang, *Phys. Rev. B*, 2001, **63** 245407; *ibid*, 2001, **63**, 121104.

38 D.Waldron, P. Haney, B. Larade, A. MacDonald, and H. Guo, *Phys.Rev. Lett.*, 2006, **96**, 166804.

39 D. Waldron, V. Timoshevskii, Y. Hu, K. Xia, and H. Guo, *Phys. Rev. Lett.*, 2006, **97**, 226802.

40 L. Kleinman and D. M. Bylander, Phys. Rev. Lett. **48**, 1425 (1982).

41 B. G. Wang, J. Wang, and H. Guo, *J. Phys. Soc. Jpn.*, 2001, **70**, 2645.

42 In our numerical calculation, k points are mostly sampled in the sharp cone regime of the first Brillouin zone as shown in Fig.3(a)-(d). The other k points do not contribute to the transient current.

43 Note that Γ_0 here is related but not directly equal to the line-width function $\Gamma_{\alpha k}$.

44 J.L. D'Amato, and H.M. Pastawski, *Phys. Rev. B*, 1990, **41**, 7411.

45 B.C. Stipe, M.A. Rezaei, W. Ho, *Science*, 1998, **280**, 1732.

46 N. Sergueev, D. Roubtsov, H. Guo, *Phys. Rev. Lett.*, 2005, **95**, 146803; N. Sergueev, A.A. Demkov, H. Guo, *Phys. Rev. B*, 2007, **75**, 233418.

47 M. Buttiker, *Phys. Rev. B*, 1986, **33**, 3020.

48 R. Golizadeh-Mojarad and S. Datta, *Phys. Rev. B*, 2007, **75**, 081301R.

49 Jesse Maassen, Ferdows Zahid, and Hong Guo, *Phys. Rev. B*, 2009, **80**, 125423.

50 Moumita Dey, Santanu K. Maiti, S.N. Karmakar, *Organic Electronics*, 2011, **12**, 1017.

51 Y.Q. Ke, K. Xia, and H. Guo, *Phys. Rev. Lett.*, 2008, **100**, 166805; *ibid*, 2010, **105**, 236801; D.P. Liu, X.F. Han, and H. Guo, *Phys. Rev. B*, 2012 **85**, 245436.